

Coverage and Spectral Efficiency of Indoor mmWave Networks with Ceiling-Mounted Access Points

Fadhil Firyaguna, Jacek Kibilda, Carlo Galiotto, Nicola Marchetti
CONNECT Centre, Trinity College Dublin, Ireland
{firyaguf, kibildj, galiotc, nicola.marchetti}@tcd.ie

Abstract—Provisioning of high throughput millimetre-wave signal to indoor areas that potentially serve a large number of users, such as transportation hubs or convention centres, will require dedicated indoor millimetre-wave access point deployments. In this article, we study dense deployments of millimetre-wave access points mounted on the ceiling, and illuminating selected spots on the ground with the use of fixed directional antennas. In this setup, the main factor limiting signal propagation are blockages by human bodies. We evaluate our system under a number of scenarios that take into account beamwidth of the main-lobe, access point density, and positioning of the mobile device with respect to the user's body. We find that both coverage and area spectral efficiency curves exhibit non-trivial behaviour which can be classified into four regions related to the selection of access point density, beamwidth, and height values. Furthermore, we observe a trade-off in beamwidth design, as the optimal beamwidth maximizes either coverage or area spectral efficiency, but not both. Finally, when we consider different body shadowing scenarios, our network design optimizes coverage or area spectral efficiency performance towards either devices held in hand or worn directly against the body, as each of the scenarios requires mutually exclusive settings of access point density and beamwidth.

Keywords—millimetre-wave networks, ultra-dense networks, self-body blockage.

I. INTRODUCTION

According to the taxonomy provided by ETSI [1], millimetre-wave (mmWave) spectrum spans frequencies from 50 GHz to 300 GHz. Systems that could provide reliable communications over these frequencies attract great attention as the said frequencies offer much wider bandwidths at shorter wavelengths, in comparison to micro-wave frequencies. While wider bandwidth may be directly translated to increased link throughput, the shorter wavelength may allow networks to take greater advantage of techniques that increase power concentration at the receiver and spatial separation between the transmitters, resulting in capacity gains. Coarse estimates provided by ETSI show that, even with a single-antenna, a 500 MHz 16-QAM mmWave link may achieve over 1 Gbps of throughput. This signifies that, if mmWave systems are shown to be technically and commercially feasible, they could be used to address the capacity objectives of 5G.

Yet, cellular systems that utilize mmWave frequencies will likely be providing coverage that is confined to streets and, more generally, outdoor areas only, as mmWave signals do not propagate well through physical objects [2]. This creates

a situation in which an independent tier of mmWave access points (APs) would be required to ensure even basic coverage over indoor areas that serve potentially large number of end users, such as concert halls, transportation hubs, or convention centres.

State-of-the-art literature on mmWave communications has shown that mmWave deployments can be a source of high bit-rate signal for indoor users (see, for example, [3], [4]) but, as we will discuss in the following section, it has not provided much in the way of network-level design and radio access infrastructure deployment. In this paper we close this gap by studying the performance effects of deployment densification of ceiling-mounted mmWave access points with highly directional antennas over a confined area.

In our scenario mmWave access points are mounted on the ceiling or walls to form a grid-like pattern and set to illuminate selected spots on the ground. In this case, and given the significantly shorter distances between the APs and user equipments (UEs) than in an outdoor scenario, the main factor limiting signal propagation are blockages by human bodies, which have been shown to introduce as much as 40 dB of attenuation to the propagating mmWave signal (see, for example, [5], [6]). Moreover, the potential lack of fixed physical obstructions such as inner-walls may result in interference between adjacent APs, despite the usage of directional transmissions. Effectively, deploying such networks requires understanding of the relationship between basic design parameters such as AP density, main lobe width, or transmit power and the propagation features of mmWave signals.

What we find is that both the coverage and area spectral efficiency (ASE) curves display non-trivial behaviour which can be classified into four regions related to the selection of AP density, beamwidth and height values. Furthermore, we find that there is a trade-off in beamwidth design, as the optimal beamwidth maximizes either coverage or ASE, but not both. This trade-off gets more complicated when we consider an indoor mmWave scenario where human body introduces significant attenuation to the propagating signal which cannot be fully compensated for with handovers (as we show in the analysis of the cell association policy). To better understand this we compare the coverage and ASE for two scenarios of human body shadowing: a UE operated in front of the user ("UE in hand") and a UE located in the pocket or carried as a wearable ("UE in pocket"). In the former scenario, the peak coverage requires that we use denser deployment and smaller beamwidths, which is shown to be beneficial also to

the achieved ASE.¹ In the latter scenario, the peak coverage requires that we use lower deployment densities and larger beamwidths, although this configuration is not optimal for the achieved ASE.

In what follows we provide an overview of the related literature, a description of our system model, and an in-depth analysis of the numerical results obtained, with lessons learnt on the design of dense indoor mmWave networks.

II. RELATED WORK

Our goal is to study the performance effects of deployment densification of ceiling-mounted mmWave access points with highly directional antennas over a confined area. While state-of-the-art literature has not addressed this topic directly, there are various other well-studied subjects, such as network densification, which provide us with relevant conclusions.

Network densification is key to increasing the capacity of conventional mobile networks, as spectrum designated for cellular communications in microwave frequencies is relatively scarce. In the mmWave frequencies, where spectrum is in abundance but adverse propagation conditions limit the signal penetration, network densification may be used to shorten the physical distance between the transmitters and receivers, ramping up the signal level at the receivers' input. Indeed, dense mmWave networks have been shown to be an attractive deployment option for outdoor urban areas [7]–[10]. In [8] it has been shown that optimal operation of a wide-area mmWave system requires a deployment that is dense enough to ensure line-of-sight conditions from at least a few transmitters. Lower density deployments result in significantly lower performance due to non-line-of-sight operation, while higher density deployments lead to an increase in interference which deteriorates the system's performance. Wide-area cellular systems based on mmWave frequency bands also require extensive indoor deployments as mmWave signals do not penetrate well majority of materials [2].

In fact, as early as 2011, WiGig in cooperation with IEEE 802.11, proposed a PHY/MAC layer that was dedicated towards wireless local area operation in mmWave frequency bands (see [11]). The proposed technology was integrated with WiFi standards operating in microwave frequency bands allowing for a graceful fallback to microwave spectrum operation when needed (see [11]). Number of research studies have confirmed the technology to be capable of delivering Gbit/s link throughputs over a range of up to 10 metres in line-of-sight conditions (see, for example, [12]). However, the network-level performance of mmWave indoor deployments, such as WiGig (or 802.11ad as it is currently known) remains largely unknown.

In a mmWave indoor scenario, characterized by much smaller distances between access points and users, the main factor limiting deployment options are blockages by physical objects such as human bodies. Human body blockage was shown to cause severe signal blockages (as high as 40 dB) that reduce the spectral efficiency gains obtained from operation

over larger bandwidths available in mmWave frequencies (see [13], [14]). In small enclosed areas this detrimental effect of body-related shadowing can be at least partially mitigated by application of reflective materials to vertical surfaces and usage of signal relays (see [3], [15]). However, in large open indoor areas these may not necessarily be available and, moreover, lack of fixed physical obstructions such as walls may actually lead to significant interference between adjacent access points requiring that the mmWave link performance is considered from network-level perspective. In [16] the trade-off between the received signal strength and the probability of blockage when deciding on the transmit antenna height is reported. Simply shortening the distance to the receiver by lowering antenna heights (thereby reducing distance-dependent pathloss) yields a greater chance of the signal being blocked by the human body, especially in crowded areas [3], [17]. This trade-off can be exploited to study optimal altitude for signal-providing low altitude platforms [18], such as quadcopters, or balloons, or urban outdoor cellular deployments with blockages from human bodies [19]. Furthermore, as it was shown in [9], increase in human body blockage loss increases “coverage inequality” in the system, as receivers with poor coverage observe a further reduction to coverage, while good coverage receivers see their coverage being improved. In this scenario, whether you observe a drop or increase in coverage depends on whether the human body is shadowing more the serving transmitter (poor coverage users) or the interferers (good coverage users). In [4], which studies device-to-device indoor mmWave communications scenario, it is shown that, under the assumption of a random direction of the interferer's main-lobe, highly directional beams will be required to maintain Gbit/s links in crowded indoor areas.

Despite these detailed insights on the impact of heights, fixed beamwidths and body blockage on the performance of both conventional and mmWave links, inspected both in isolation and in the network context, still little is known about the coverage and ASE trade-offs in densification of ceiling-mounted mmWave access points. In the following, building on the state-of-the-art literature for mmWave network modelling [20], we setup a system model that allows us to inspect the trade-offs between peak coverage and ASE given variety of blockage scenarios and cell association strategies.

III. SYSTEM MODEL

The considered environment is an indoor confined area where the main obstacles for the mmWave signal propagation are human bodies, i.e., we assume a scenario with no corridors or walls such as theatres and convention centre halls. The APs are deployed on a hexagonal grid throughout the indoor venue, and they are installed on the ceiling at a height h_{AP} above the UE level, with fixed directional antennas illuminating the floor below. We consider a UE randomly located in the cell at the centre of the venue. The UE is associated with the serving AP for the downlink transmission by a given cell association strategy defined in Section IV-A.

¹The corresponding ASE achieved with the optimal beamwidth for coverage.

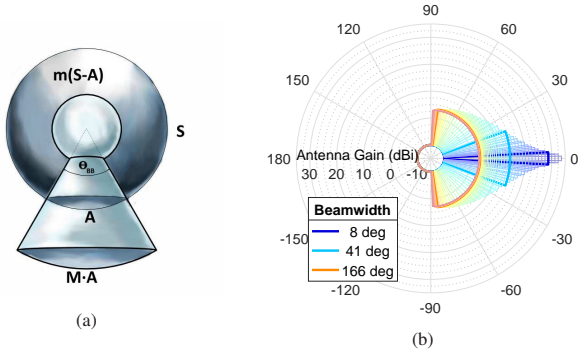


Fig. 1: (a) Cone-bulb model approximation of antenna directivity gain patterns. The cone represents the main-lobe and the bulb (inner sphere) represents the side-lobe. The cap area A is “amplified” by a factor of M , while the resulting bulb area $S - A$ is “shrunk” by a factor of m . (b) Antenna directivity gain pattern for different beamwidths.

A. Directivity Gain

We assume APs utilize directional transmission, while the UEs utilize omnidirectional reception. As in [21], the antenna pattern is approximated by a cone of uniform gain representing the main-lobe attached to a single “bulb” representing the side-lobe, as illustrated in Fig. 1a, where M is the main-lobe directivity gain, m is the side-lobe gain, θ_{BW} is the beamwidth of the main-lobe, A is the area of the spherical cap, and S is the surface area of the sphere. The directivity gains are then a function of the beamwidth, normalized over a given spherical surface as in:

$$M \cdot \frac{A}{S} + m \cdot \frac{S - A}{S} = 1, \quad (1)$$

where the area of the cap is given by $A = 2\pi r^2(1 - \cos \frac{\theta_{BW}}{2})$, and the sphere surface area is $S = 4\pi r^2$. Thus, fixing the side-lobe gain m , we can calculate the main-lobe gain as a function of the beamwidth:

$$M(\theta_{BW}, m) = \frac{2 - m(1 + \cos \frac{\theta_{BW}}{2})}{1 - \cos \frac{\theta_{BW}}{2}}. \quad (2)$$

The UE receives maximum directivity gain M of an AP when the UE is positioned in the illumination area of the main-lobe of that AP, i.e., the UE is inside the projected circle of the main-lobe of radius:

$$r_M = h_{AP} \cdot \tan \frac{\theta_{BW}}{2}, \quad (3)$$

as illustrated in Fig. 2a. Otherwise, the directivity gain is the AP side-lobe gain m (as shown in Fig. 1b).

B. Self-Body Blockage

In our scenario, the only source of blockage is a human body. Body blockage can cause up to 40 dB of attenuation to the penetrating signal [5], [6], [9], [13]. The main factor that describes the extent to which human body shadows signals to/from the UE is the UE’s position with respect to the body. This position is determined by two parameters: d_{toBody} and

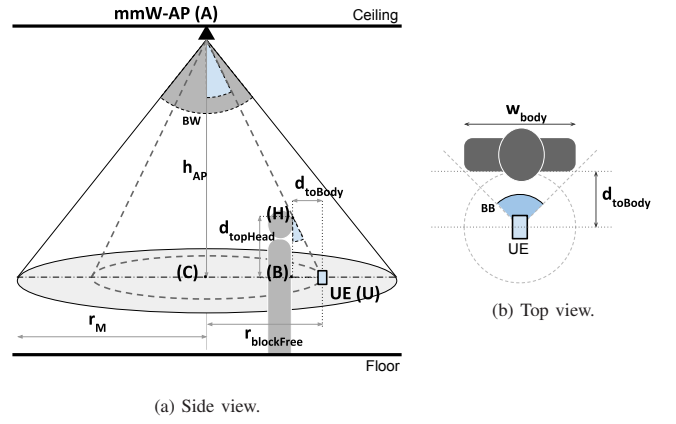


Fig. 2: Self-body blockage model. Side view (a): vertical obstruction by the user body may happen when the UE is beyond the radius $r_{blockFree}$. User is holding the UE at a distance of d_{toBody} in front of the body, and at a distance of $d_{topHead}$ to the top of the head level. Top view (b): the user body horizontally blocks a region around the UE defined by the angle θ_{BB} .

$d_{topHead}$ (as shown in Fig. 2a). The first one determines the distance to the body and how wide the signal obstruction is, e.g., zero distance could represent a scenario where the device is held in a pocket and the body obstructs half of the field of view, while a distance of 30 cm could represent a scenario where a user is browsing the Internet and the body obstructs a narrower area. The second parameter determines the amount of body obstruction in the vertical dimension. Given the body blockage and our ceiling-mounted deployments, we can construct a model of user device shadowing as depicted in Fig. 2a. From the geometry of the model, we define $r_{blockFree}$ as the radius of the *self-block free zone*:

$$r_{blockFree} = h_{AP} \cdot \frac{d_{toBody}}{d_{topHead}}, \quad (4)$$

where the UEs inside this zone are never obstructed by the user body, while the UEs outside of it are obstructed whenever the user body is between the UE and the AP. Now, assuming uniform body orientation, the probability of a user body obstructing the AP’s signal (self-block probability) is:

$$P_{BB} = \arctan \left(\frac{w_{body}}{2 \cdot d_{toBody}} \right) / \pi. \quad (5)$$

C. Signal-to-Interference-Noise Ratio

In this work, we consider the following path loss model:

$$L(d, h_{AP}) = L_0 \cdot R(d, h_{AP})^{-\alpha}, \quad (6)$$

where L_0 is the path loss at 1 metre distance under free space propagation, α is the attenuation exponent, d is the projection of the distance on the horizontal plane (2D-distance) from the cell centre to the UE, and $R(d, h_{AP})$ is the Euclidean distance from the AP to the UE.

Based on the assumptions made above, we can express the SINR at a UE as:

$$\text{SINR} = \frac{G_i \cdot L(d_i, h_{\text{AP}}) \cdot B_i}{N_0/P_{\text{TX}} + \sum_{j \in \mathcal{D} \setminus \{i\}} G_j \cdot L(d_j, h_{\text{AP}}) \cdot B_j}, \quad (7)$$

where \mathcal{D} represents the set of all APs in the system, d_i is the distance to the serving AP $i \in \mathcal{D}$, $G_i \in \{m, M\}$ is the directivity gain of AP i , $B_i \in \{L_{\text{body}}, 1\}$ is the body attenuation for the link between the reference user and AP i (L_{body} is the attenuation loss produced by the body), N_0 is the thermal noise power, and P_{TX} is the transmit power. Note that G_i and B_i are random variables whose distributions are functions of the system parameters (θ_{BW} , h_{AP} , d_{toBody} , d_{topHead} , w_{body}), and distance d_i .

In our scenario, we assume there are no physical obstructions to the propagating signal other than the user's body; in addition, we consider the reflections from ceiling and ground to be negligible, which may be considered a reasonable modelling assumption since, as reported in [22], [23], several materials used for ceiling and flooring surfaces produce a significant attenuation in the reflected signal.

IV. NUMERICAL RESULTS

A. Simulation Setup

We model our scenario by placing APs in the centres of a hexagonal cell pattern laid over a $400 \times 400 \text{ m}^2$ area, as exemplified in Fig. 3. This specific choice of the area size allows us to mitigate the edge effect, and to explore the system behaviour for longer inter-site distances. The side-lobe gain is fixed at -10 dB , and the main-lobe gain varies with the beamwidth according to Eq. (2). We evaluate the system for a fixed AP height $h_{\text{AP}} = 10 \text{ m}$. Note that, changing h_{AP} has essentially the same impact on the performance as changing the beamwidth, since both h_{AP} and θ_{BW} determine the main-lobe illumination area; as a matter of fact, when testing our system for other height values of interest, we observed no significant deviations from our conclusions. We set the attenuation exponent as $\alpha = 2$, transmit power as 20 dBm , bandwidth as 100 MHz , carrier frequency as 60 GHz , noise figure as 9 dB , we consider no small-scale fading, and we set the body parameters w_{body} as 40 cm and d_{topHead} as 40 cm . We set the parameter d_{toBody} to define different blockage scenarios: $d_{\text{toBody}} = 30 \text{ cm}$ represents a scenario of a user operating the UE with the *hand* (UE in hand), and $d_{\text{toBody}} = 0 \text{ cm}$,² represents a scenario of the UE held in *pocket* (UE in pocket). The UE is associated with an AP that provides it with a downlink signal according to either the shortest 3D Euclidean distance (*minimum distance association*) or the strongest received signal power (*maximum received power association*). The simulation source code is available on-line (see Appendix A).

²In this scenario, $r_{\text{blockFree}}$ equals 0, according to Eq. 4, and there is no self-block free zone.

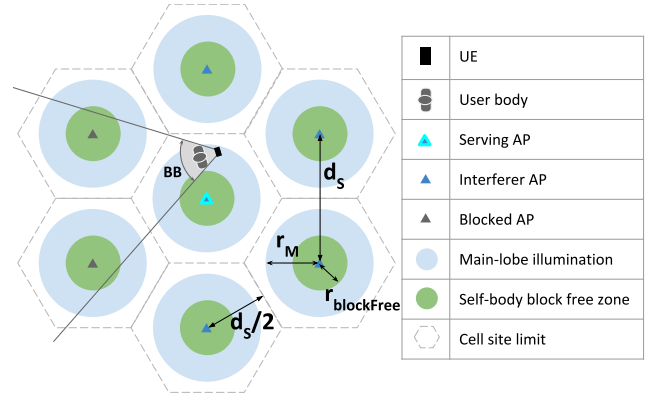


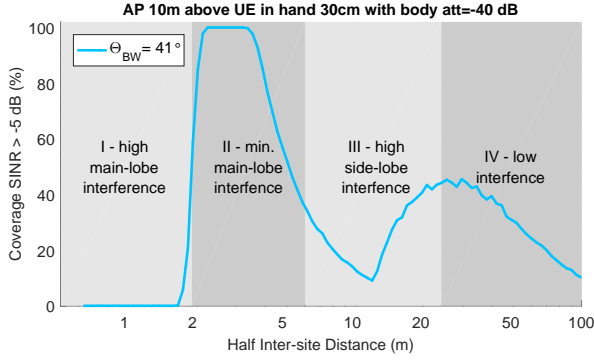
Fig. 3: Snapshot from simulations illustrating the system model. The APs are distributed according to a hexagonal cell pattern with an inter-site distance d_s . User body is blocking the signal from the gray-colored APs. The UE is illuminated (light-blue area) by the serving AP and is not within the self-block free zone (green area). Note that in a very dense topology, where d_s could be as small as $r_{\text{blockFree}}$, the site area could correspond to self-block free zone.

B. Coverage and Area Spectral Efficiency Profile

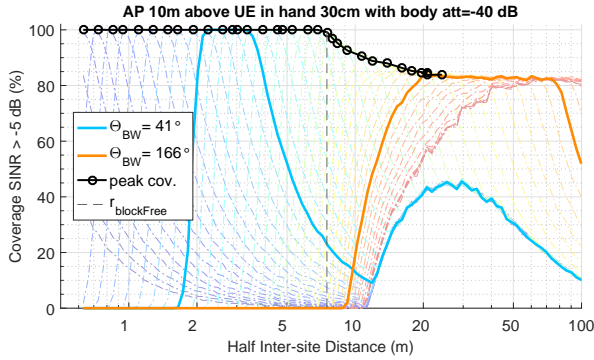
In this subsection, we evaluate the effect of the inter-site distance (network density) and beamwidth on coverage and area spectral efficiency (ASE) of a mmWave indoor network with ceiling-mounted APs. The SINR coverage is defined as the probability that the SINR at the receiver is larger than some threshold T , i.e., $P[\text{SINR} > T]$, while the ASE is the spectral efficiency $\log(1 + \text{SINR})$ averaged over all realizations, and divided by the cell area. The results for coverage and ASE are shown in Fig. 4b and 4c, respectively; for now, we focus on the minimum distance cell association case.

Our investigation reveals that, in the ceiling-mounted AP setup, the SINR coverage presents a non-trivial behaviour which can be classified into four regions, as illustrated in Fig. 4a. These appear as we change the inter-site distance while keeping the beamwidth fixed: (i) **high main-lobe interference**: at high AP density (short d_s), the beam is too large and causes substantial overlaps among adjacent cells, which results in high interference and, thus, low coverage; (ii) **minimum main-lobe interference**: the main-lobe illuminates the entire cell with minimum interference to neighbouring cells, yielding high coverage; from this point on, as we move towards a sparser deployment, the cell size becomes larger than the illuminated area and the coverage is inevitably reduced; (iii) **high side-lobe interference**: at intermediate AP densities, the coverage is very low due to the lack of main-lobe illumination by the serving AP and due to high neighbour side-lobe interference; however, this interference decreases as the deployment gets sparser, leading to increased coverage; (iv) **low interference**: in low AP density (large d_s), the beam is so small that it becomes negligible; therefore, the only signal that can be picked-up by the majority of users comes from the side-lobe and is thus weak enough for the noise to dominate the SINR term.

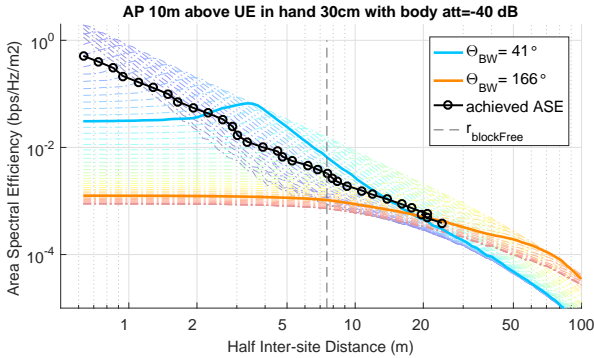
Based on these results, it is clear that for each cell size (or each AP density) there is an optimal design of beamwidth that leads to a peak coverage, which is depicted by the black line in



(a) Regions delimited by gray rectangles represents the non-trivial behaviour of coverage in the selected AP density.



(b) Coverage for SINR threshold above -5 dB.



(c) Area spectral efficiency.

Fig. 4: Coverage and ASE for different beamwidths (light and dotted lines) when the user holds the UE in hand and the APs are mounted 10 m above the UE. The results for beamwidths of 41° and 166° are pictured in solid lines. The black line in (a) is the interpolation of the maximum coverage achieved for a given beamwidth and inter-site distance. The black line in (b) is the ASE achieved from choosing a given pair beamwidth/inter-site distance. The gray vertical dashed line is the radius of the self-block free zone.

Fig. 4b. For example, the half inter-site distance $d_S/2 \approx 3.4$ m corresponds to peak coverage when $\theta_{BW} = 41^\circ$ (which is equivalent to the main-lobe radius $r_M = 3.7$ m). It should be noted that the optimal beamwidth for -5 dB coverage does not optimize the ASE. As we see from the black line in Fig. 4c, the achieved ASE is lower than the maximum achievable

for a given inter-site distance. A more detailed discussion of this trade-off between coverage and ASE is presented in Section IV-D.

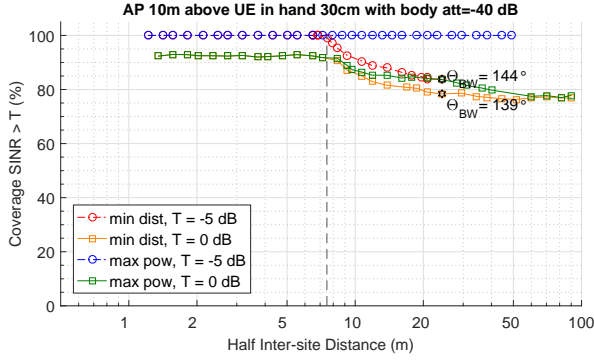
With reference to Fig. 4b, the fact that we observe high peak coverage at high AP densities and relatively lower coverage at lower AP densities depends on whether the cell size is smaller than the self-block free zone; one should note that when the cell size is smaller than the self-block free zone (on the left of the dashed line in Fig. 4b), all UEs are free from self-blockage, leading to high peak coverage. On the other hand, when the cell is bigger than the self-block free zone (on the right of the dashed line), there are some UEs outside the self-block free zone that will be blocked by the body with probability P_{BB} , according to Eq. 5. These UEs will have their SINR degraded by the body attenuation, increasing the number of UEs whose SINR is below the threshold. Hence, the coverage will decrease proportionally to the number of blocked UEs.

C. Cell Association and Body Blockage

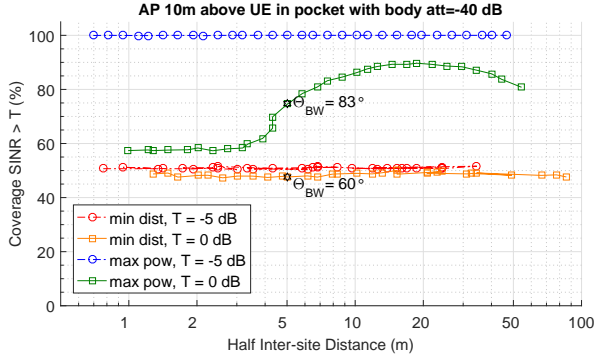
In this subsection, we investigate the impact of UE-to-AP association on peak coverage. To that end, we compare two different association strategies, namely *minimum distance* and *maximum received power* (as defined in Section IV-A) and we consider two different scenarios of interest, i.e., UE in hand — which represents a typical device usage — and UE in pocket — which represents a severe blockage scenario. The corresponding results are shown in Fig. 5a and 5b, respectively. First, it is important to remark that the maximum received power association strategy leads to larger optimal beamwidths compared to the minimum distance strategy, meaning that it yields a cellular deployment with larger overlaps between adjacent AP main-lobes. For example, in Fig. 5b, for $d_S/2 = 5.02$ m and $T = 0$ dB, the maximum received power association (green line) leads to the optimal beamwidth of 83° (UE in pocket), while the minimum distance association (orange line) leads to the optimal beamwidth of 60° . Second, our results show that, as expected, maximum power association strategy generally improves the coverage of the network.

In addition, there are a few minor observations that can be made. First, in the UE in pocket scenario, with the minimum distance strategy, the coverage achieves approximately 50%. This is because in this scenario, the probability of blockage P_{BB} is 50%, which means that half of the users will block the signal to their UE, attenuating the signal by 40 dB. Since, in the minimum distance strategy, the blocked UEs will not associate with another AP, those users will have a poor SINR, leading to approximately 50% of the users not being covered. Second, the coverage can be improved with the maximum received power strategy because those 50% of users will associate with another AP and will have a better SINR. Nonetheless, this improvement depends on the SINR threshold. For example, with $T = -5$ dB, we have 100% coverage at any AP density (see blue curve in Fig. 5b), whereas with $T = 0$ dB, the coverage is lower than in the former case (up to 90%)³ and

³Even with the maximum received power association, the 0 dB threshold coverage does not reach 100% in any of the body shadowing scenarios we have taken into account (an observation which coincides with the one made in [9]).



(a) UE in hand.



(b) UE in pocket.

Fig. 5: Comparison of peak coverage for different SINR thresholds for two cell association strategies: minimum distance (red/orange curves) and maximum received power (blue/green curves). Optimal θ_{BW} , for a given d_S (black marks), is generally larger when using maximum power association.

presents a drop for high AP densities (as we can see from the green curve in Fig. 5b for half inter-site distances below 5m). The reason for this particular behaviour of the green curve in Fig. 5b is the following. At high AP densities, the SINR of the majority of the UEs is low (in particular, lower than the threshold) because of the strong interference from neighbouring APs, which is caused by the short distances between these APs and the UE, and by high directivity gains (i.e., we recall that, at high AP densities, we obtain small optimal beamwidths and thus high antenna directivity gains). Therefore, the SINR values of those UEs degrade the coverage to approximately 58%; even so, this represents an improvement compared to the minimum distance strategy case.

In light of these results, for the UE in pocket scenario, it is important to consider an association strategy that allows for the mitigation of body shadowing effect, so as to provide satisfactory coverage. This is not the case for UEs in hand, as in this case the body shadowing effect on coverage is not as severe (as we can see by comparing the gains of the maximum received power association from Fig. 5a and Fig. 5b).

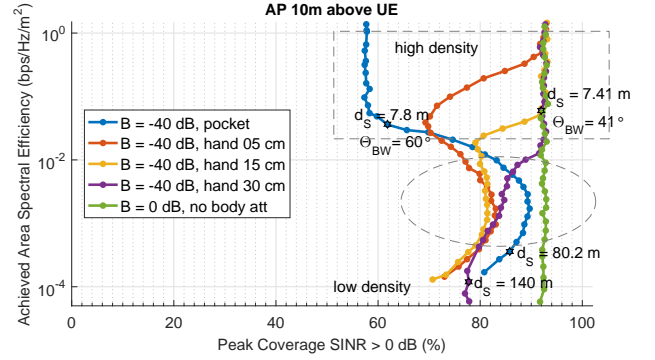


Fig. 6: Trade-off between peak coverage (obtained for optimal beamwidth) and achieved ASE for different body attenuation scenarios. Inter-site distance increases from the upper points to the lower ones. The UE associates with the AP with maximum received power. UE in pocket scenario needs larger beamwidths to achieve peak coverage. Points inside the rectangle provides best trade-off for UE in hand scenario. Points inside the ellipse provide best coverage for UE in pocket scenario and not lower ASE than inside the rectangle.

D. ASE vs. Coverage Trade-off

Finally, we analyzed the trade-off between the peak coverage and the achieved ASE and its behaviour for different body shadowing scenarios and for different AP densities. We investigate this trade-off for the SINR threshold of 0 dB, which represents the UEs with higher receiver sensitivity; we focus on these UEs because they provide us with better insight on how the density and beamwidth settings affect network performance. The results are shown in Fig. 6: each point of the curve corresponds to the optimal beamwidth θ_{BW} for a given inter-site distance d_S when using maximum power association. The lower points in the figure represent the ASE/coverage for larger θ_{BW} and lower AP density (longer d_S), while the upper points represent the ASE/coverage for smaller θ_{BW} and higher AP density (shorter d_S). The main observation we make is that coverage and ASE in the UE in pocket scenario require different optimal beamwidth and AP densities. For example, to optimize the coverage vs. ASE trade-off in hand scenarios, the network should be designed to be dense and to use small beamwidths, i.e., choosing the points inside the gray rectangle of Fig. 6, where the coverage is around 90% and the ASE is close to 1 bps/Hz/m². However, the same configuration would yield poor coverage for UEs that are held in pocket.

A different design approach aiming at coverage maximization for the UE in pocket scenario requires deploying a sparser network with larger beamwidths (see points inside the ellipse Fig. 6). However, this design criterion is not optimal from the perspective of ASE; as shown in the plot, ASE suffers two orders of magnitude reduction as compared to the optimal value achievable with a denser network.

To summarize, we can optimize the design of indoor ceiling-mounted AP mmWave networks either for the UE in hand scenario or for the UE in pocket scenario, but not both, as each scenario has different optimal configurations.

V. CONCLUSION

Herein we studied the performance effects of deployment densification of ceiling-mounted mmWave access points with highly directional antennas over a confined area. We showed that, while being feasible, dense indoor mmWave deployments have their intrinsic characteristics, which make it necessary for network designers to decide (and understand) what is their intended end user. First, the optimal choice of beamwidth maximizes either coverage or ASE, but not both. Second, how this trade-off manifests itself will also depend on the human body shadowing scenario, i.e., the distance between the receiver and the potential obstruction, as the optimal choice of beamwidth and AP density corresponds to the body blockage probability. As pointed out in Section IV-A, it is worth emphasizing that these findings are consistent across a range of area sizes and AP heights relevant to the type of scenario we are considering.

Still more work is needed to understand how these trade-offs change when the mmWave signals are scattered and reflected by the indoor environment. However, even the results we have so far can be readily used to inform the design of interference coordination techniques based on beam-steering, or new hand-off and cell association procedures that account for potential body shadowing of mmWave signals.

ACKNOWLEDGMENT

This publication has emanated from the research conducted within the scope of *NEMO (Enabling Cellular Networks to Exploit Millimeter-wave Opportunities)* project financially supported by the Science Foundation Ireland (SFI) under Grant No. 14/US/I3110 and with partial support of the European Regional Development Fund under Grant No. 13/RC/2077.

APPENDIX A

All simulation scripts used to generate the presented results were written in MATLAB® and can be cloned from the following repository:

<https://github.com/firyaguna/matlab-nemo-mmWave>

REFERENCES

- [1] European Telecommunications Standards Institute, "millimetre Wave Transmission (mWT): Applications and Use Cases of Millimetre Wave Transmission," European Telecommunications Standards Institute, Tech. Rep. ETSI GS mWT 002 v1.1.1, Aug. 2015. [Online]. Available: <http://www.etsi.org>
- [2] Z. Pi and F. Khan, "An Introduction to Millimeter-Wave Mobile Broadband Systems," *IEEE Communications Magazine*, vol. 49, no. 6, pp. 101–107, Jun. 2011.
- [3] K. Dong, X. Liao, and S. Zhu, "Link Blockage Analysis for Indoor 60GHz Radio Systems," *Electronics Letters*, vol. 48, no. 23, pp. 1506–1508, Nov. 2012.
- [4] K. Venugopal, M. C. Valenti, and R. W. Heath, "Device-to-Device Millimeter Wave Communications: Interference, Coverage, Rate, and Finite Topologies," *IEEE Transactions on Wireless Communications*, vol. 15, no. 9, pp. 6175–6188, Sep. 2016.
- [5] S. Collonge, G. Zaharia, and G. E. Zein, "Influence of the Human Activity on Wide-Band Characteristics of the 60 GHz Indoor Radio Channel," *IEEE Transactions on Wireless Communications*, vol. 3, no. 6, pp. 2396–2406, Nov. 2004.
- [6] S. Rajagopal, S. Abu-Surra, and M. Malmirchegini, "Channel Feasibility for Outdoor Non-Line-of-Sight mmWave Mobile Communication," in *2012 IEEE Vehicular Technology Conference (VTC Fall)*, Sep. 2012, pp. 1–6.
- [7] T. Bai and R. W. Heath, "Coverage Analysis for Millimeter Wave Cellular Networks with Blockage Effects," in *2013 IEEE Global Conference on Signal and Information Processing (GlobalSIP)*, Dec. 2013, pp. 727–730.
- [8] —, "Coverage in Dense Millimeter Wave Cellular Networks," in *2013 47th Asilomar Conference on Signals, Systems and Computers*. IEEE, Nov. 2013, pp. 2062–2066.
- [9] —, "Analysis of Self-Body Blocking Effects in Millimeter Wave Cellular Networks," in *2014 48th Asilomar Conference on Signals, Systems and Computers*. IEEE, Nov. 2014, pp. 1921–1925.
- [10] —, "Coverage and Rate Analysis for Millimeter-Wave Cellular Networks," *IEEE Transactions on Wireless Communications*, vol. 14, no. 2, pp. 1100–1114, Feb. 2015.
- [11] C. J. Hansen, "WiGiG: Multi-Gigabit Wireless Communications in the 60 GHz Band," *IEEE Wireless Communications*, vol. 18, no. 6, pp. 6–7, Dec. 2011.
- [12] X. Zhu, A. Doufexi, and T. Kocak, "Throughput and Coverage Performance for IEEE 802.11ad Millimeter-Wave WPANs," in *2011 IEEE 73rd Vehicular Technology Conference (VTC Spring)*, May 2011, pp. 1–5.
- [13] J. S. Lu *et al.*, "Modeling Human Blockers in Millimeter Wave Radio Links," *ZTE Communications*, vol. 10, no. 4, pp. 23–28, 2012.
- [14] T. S. Rappaport *et al.*, "Millimeter Wave Mobile Communications for 5G Cellular: It Will Work!" *IEEE access*, vol. 1, pp. 335–349, 2013.
- [15] C. S. Leong *et al.*, "A Robust 60 GHz Wireless Network with Parallel Relaying," in *2004 IEEE International Conference on Communications (ICC)*, vol. 6, Jun. 2004, pp. 3528–3532.
- [16] J. Wells, "Faster than Fiber: The Future of Multi-G/s Wireless," *IEEE Microwave Magazine*, vol. 10, no. 3, May 2009.
- [17] K. Venugopal, M. C. Valenti, and R. W. Heath, "Analysis of Millimeter Wave Networked Wearables in Crowded Environments," in *2015 49th Asilomar Conference on Signals, Systems and Computers*. IEEE, Nov. 2015, pp. 872–876.
- [18] A. Al-Hourani, S. Kandeepan, and S. Lardner, "Optimal LAP Altitude for Maximum Coverage," *IEEE Wireless Communications Letters*, vol. 3, no. 6, pp. 569–572, Dec. 2014.
- [19] M. Gapeyenko *et al.*, "Analysis of Human-Body Blockage in Urban Millimeter-Wave Cellular Communications," in *2016 IEEE International Conference on Communications (ICC)*, May 2016, pp. 1–7.
- [20] J. G. Andrews *et al.*, "Modeling and Analyzing Millimeter Wave Cellular Systems," *IEEE Transactions on Communications*, vol. 65, no. 1, pp. 403–430, Jan. 2017.
- [21] R. Ramanathan, "On the Performance of Ad Hoc Networks with Beamforming Antennas," in *Proceedings of the 2nd ACM International Symposium on Mobile Ad Hoc Networking & Computing*, Oct. 2001, pp. 95–105.
- [22] C. Yiu and S. Singh, "Empirical Capacity of mmWave WLANs," *IEEE Journal on Selected Areas in Communications*, vol. 27, no. 8, pp. 1479–1487, 2009.
- [23] Z. Genc *et al.*, "Robust 60 GHz Indoor Connectivity: Is It Possible with Reflections?" in *2010 IEEE 71st Vehicular Technology Conference (VTC Spring)*, Sep. 2010, pp. 1–5.